

ipole - semianalytic scheme for relativistic polarized radiative transport

M. Mościbrodzka¹★, C.F. Gammie²†

¹*Department of Astrophysics/IMAPP, Radboud University, P.O. Box 9010, 6500 GL Nijmegen, The Netherlands*

²*Department of Astronomy and Department of Physics, University of Illinois, Urbana, IL 61801, USA*

Accepted XXX. Received YYY; in original form ZZZ

ABSTRACT

We describe `ipole`, a new public ray-tracing code for covariant, polarized radiative transport. The code extends the `ibothros` scheme for covariant, unpolarized transport using two representations of the polarized radiation field: in the coordinate frame, it parallel transports the coherency tensor; in the frame of the plasma it evolves the Stokes parameters under emission, absorption, and Faraday conversion. The transport step is implemented to be as spacetime- and coordinate- independent as possible. The emission, absorption, and Faraday conversion step is implemented using an analytic solution to the polarized transport equation with constant coefficients. As a result, `ipole` is stable, efficient, and produces a physically reasonable solution even for a step with high optical depth and Faraday depth. We show that the code matches analytic results in flat space, and that it produces results that converge to those produced by Dexter’s `grtrans` polarized transport code on a complicated model problem. We expect `ipole` will mainly find applications in modeling Event Horizon Telescope sources, but it may also be useful in other relativistic transport problems such as modeling for the IXPE mission.

Key words: black hole physics – MHD – polarization – radiative transfer – relativistic processes

1 INTRODUCTION

The Event Horizon Telescope (EHT) will soon produce full polarization images of the luminous plasma surrounding the event horizon in the low accretion rate systems Sgr A* and M87* (Johnson et al. 2015). Much of the information content of EHT observations will be in the polarized components of the radiation field; extracting this information will require a model for the state of the radiating plasma as well as the ability to produce mock full polarization observations of these models. Although mock total intensity observations of accretion flow and jet models have now become common (Falcke et al. 2000; Noble et al. 2007; Broderick et al. 2009; Broderick & Loeb 2009a; Dexter & Agol 2009; Mościbrodzka et al. 2009; Yuan et al. 2009; Dexter et al. 2010; Broderick et al. 2011a,b; Dexter & Fragile 2011; Vincent et al. 2011; Dexter et al. 2012; Dolence et al. 2012; Mościbrodzka et al. 2012; Younsi et al. 2012; Dexter & Fragile 2013; Chan et al. 2013; Mościbrodzka et al. 2014; Chan et al. 2015;

Vincent et al. 2015; Younsi & Wu 2015; Ball et al. 2016; Fraga-Encinas et al. 2016; Mościbrodzka et al. 2016; Pu et al. 2016a,b; Chan et al. 2017; Mao et al. 2017; Medeiros et al. 2017; Porth et al. 2017; Shiokawa et al. 2017; Roelofs et al. 2017), full polarization models – although not completely novel (Bromley et al. 2001; Broderick & Blandford 2004; Broderick & Loeb 2005; Huang et al. 2008; Shcherbakov et al. 2012; Gold et al. 2016; Mościbrodzka et al. 2017) – are less well explored.

In EHT target models millimeter photons are produced by synchrotron emission. It is therefore natural that EHT targets have substantial linear polarization, and indeed the linear polarization fraction in Sgr A* is ~ 7 per cent¹ (Bower et al. 2003, 2005; Marrone et al. 2007, 2008) and in M87 it is < 1 per cent (Kuo et al. 2014). Circular polarization can also be produced in emission and by Faraday conversion of linearly polarized radiation. The circular polarization fraction in Sgr A* has been measured as 1.2–1.6

★ E-mail: m.moscibrodzka@astro.ru.nl

† E-mail: gammie@illinois.edu

¹ It is worth mentioning that NIR emission from Sgr A* also has strong linear polarization, of 20–40 per cent (Eckart et al. 2008; Shahzamanian et al. 2015).

per cent (Muñoz et al. 2009, 2012). Our interest in polarized models is therefore well motivated.

Total intensity models of accreting black holes manifest familiar relativistic effects (Cunningham & Bardeen 1973; Cunningham 1975): gravitational lensing, doppler shift, doppler boosting, and gravitational redshift all contribute at order unity to models of accretion flows where the bulk of the emission is generated close to the event horizon. To this, full polarization models add “gravitational Faraday rotation” (Balazs 1958), i.e. the spacetime can rotate the plane of polarization of an electromagnetic wave. In the weak field limit, the rotational angle is proportional to the line of sight component of the angular momentum of the lensing mass (Ishihara et al. 1988).

Several existing codes are capable of generating polarized images of radiating plasma near a compact object.² Of these, only Dexter’s `grtrans` code (Dexter 2016) has been publicly released. It seems to us that it is useful to have multiple, distinct, publicly available solutions of the problem, for verification purposes. Nevertheless, our code is not completely independent and owes much to the careful testing and thoughtful construction of `grtrans`.

Still, our scheme differs from `grtrans` in three significant respects.

First, in the formulation of the Liouville operator (the convective derivative operator in phase space): we use parallel transport of a coherency or photon density tensor rather than direct integration of the invariant Stokes parameters with a rotation term for linear polarization. The coherency matrix approach, analogous to that developed by van Ballegooijen (1985), seems conceptually cleaner to us and requires relatively little thought (and therefore reduces the scope for error in, for example, formulating a polarization measurement). It is also manifestly covariant, so it is easy to change coordinate systems.

Second, at each step we use an analytic solution for polarized transport with constant absorption, emission, and rotation coefficients (defined below). The solution was first written down by Landi Degl’Innocenti & Landi Degl’Innocenti (1985). We recount it below, as well as a few special cases in an appendix. The result is a cheap second-order scheme that behaves well even when the absorption optical depth and/or Faraday depth is large over a single step.

Third, we directly integrate the geodesic equation rather than using `geokerr` (Dexter & Agol 2009), which relies on integrability of geodesics in the Kerr metric. Again, this makes our code coordinate and spacetime independent. We can therefore study polarization properties of non-GR black hole models, and switch to unconventional coordinate systems (such as the Cartesian Kerr-Schild coordinates used by, e.g., BHAC code, Porth et al. 2017) for the geodesic integration.

In the end, the value of each of these differences is somewhat subjective. What is not subjective is the value of having quasi-independent schemes for solving a complicated, technically demanding problem like relativistic polarized radiative transport.

² Polarized transport schemes already exist for applications in cosmology, but typically do not use ray-tracing.

This paper is organized as follows. In section 2 we present the equations of polarized radiative transfer through magnetized plasma. Section 2 outlines the coherency tensor formalism of Gammie & Leung (2012), however we also clarify a few points from that paper. In section 3, we describe a semi-analytic scheme for solving the equations in arbitrary geometry. In section 4, we present a few simple tests and demonstrate the performance of the numerical scheme in recovering known analytic solutions of the polarized transfer equations. In case of more complex problems, that do not have analytic solutions, we compare `ipole` numerical results to the results obtained with `grtrans`. We summarize the paper and conclude in section 5.

2 GOVERNING EQUATIONS

The radiative transfer equation for time-independent, unpolarized, nonrelativistic transport, including emission and absorption but not scattering, is

$$\frac{dI_\nu}{ds} = j_\nu - \alpha_\nu I_\nu, \quad (1)$$

where $I_\nu \equiv$ specific intensity, $\nu \equiv$ frequency, $j_\nu \equiv$ emissivity, and $\alpha_\nu \equiv$ absorptivity. Each term is frame dependent. The covariant generalization is

$$\frac{d}{d\lambda} \left(\frac{I_\nu}{v^3} \right) = \left(\frac{j_\nu}{v^2} \right) - (\nu \alpha_\nu) \left(\frac{I_\nu}{v^3} \right), \quad (2)$$

where $\lambda \equiv$ the affine parameter along a photon trajectory, $d/d\lambda$ is the convective derivative in phase space (“Liouville operator”), and each term in parentheses is invariant and can thus be evaluated in any frame. The affine parameter is defined through the geodesic equations

$$\frac{dx^\mu}{d\lambda} = k^\mu \quad (3)$$

and

$$\frac{dk^\mu}{d\lambda} = -\Gamma_{\alpha\beta}^\mu k^\alpha k^\beta, \quad (4)$$

where $k^\mu \equiv$ wave four-vector and $\Gamma \equiv$ connection coefficients. The frequency measured by an observer with four-velocity u^μ is

$$\omega = -k^\mu u_\mu. \quad (5)$$

The relationship between ω and the frequency in Hz measured by the observer depends on the units of k^μ . We have implicitly assumed (and will continue to assume below) that photons travel along null geodesics and therefore that ν is large compared to the plasma frequency and electron gyrofrequency (see Broderick & Blandford 2004, for a more general treatment). In EHT sources this is an excellent approximation.

The radiative transfer equation for *polarized*, time-independent, nonrelativistic transport, including emission and absorption but not scattering, is

$$\frac{d}{ds} \begin{pmatrix} I_\nu \\ Q_\nu \\ U_\nu \\ V_\nu \end{pmatrix} = \begin{pmatrix} j_{\nu,I} \\ j_{\nu,Q} \\ j_{\nu,U} \\ j_{\nu,V} \end{pmatrix} - \begin{pmatrix} \alpha_{\nu,I} & \alpha_{\nu,Q} & \alpha_{\nu,U} & \alpha_{\nu,V} \\ \alpha_{\nu,Q} & \alpha_{\nu,I} & \rho_{\nu,V} & -\rho_{\nu,U} \\ \alpha_{\nu,U} & -\rho_{\nu,V} & \alpha_{\nu,I} & \rho_{\nu,Q} \\ \alpha_{\nu,V} & \rho_{\nu,U} & -\rho_{\nu,Q} & \alpha_{\nu,I} \end{pmatrix} \begin{pmatrix} I_\nu \\ Q_\nu \\ U_\nu \\ V_\nu \end{pmatrix}, \quad (6)$$

where $I_\nu, Q_\nu, U_\nu, V_\nu$ are (frame-dependent) specific intensities associated with the Stokes parameters.³ Notice that Q_ν, U_ν, V_ν are signed quantities while I_ν is positive definite. $Q_\nu > 0$ corresponds to linear polarization along one axis in the plane perpendicular to the wave 3-vector, while $Q_\nu < 0$ corresponds to linear polarization along the second axis. U_ν describes polarization at $\pm 45^\circ$ to the first axis. V_ν is circular polarization. Positive V_ν always means right-hand circular polarization (RCP). The IEEE convention is that for RCP the electric field vector rotates in a right-handed direction at a fixed position if thumb points along wavevector k^μ . For RCP the field rotates counter-clockwise as seen from the observer (see Hamaker & Bregman 1996, for a discussion)

Equation (6) has 11 transfer coefficients that depend on physical conditions in the plasma. These are the four emission coefficients $j_{\nu,A}$ (subscript A can be one of I, Q, U, V); the four absorption coefficients $\alpha_{\nu,A}$, and the three rotation coefficients $\rho_{\nu,A}$. By definition $I_\nu^2 \geq Q_\nu^2 + U_\nu^2 + V_\nu^2$, i.e. the polarization fraction is $\leq 100\%$, and evidently we must have

$$j_{\nu,I}^2 > j_{\nu,Q}^2 + j_{\nu,U}^2 + j_{\nu,V}^2 \quad (7)$$

to guarantee this. Notice that $j_{\nu,I} > 0$, but $j_{\nu,Q}, j_{\nu,U}, j_{\nu,V}$ can have either sign. Assuming maser action is absent, $\alpha_{\nu,I} > 0$, but $\alpha_{\nu,Q}, \alpha_{\nu,U}, \alpha_{\nu,V}$ can also have either sign.

The covariant generalization of (6) is not as simple as for the unpolarized transfer equation because the definition of Q_ν, U_ν depend on the orientation of the axes by the observer who makes the measurement. Broderick & Blandford (2004) have presented a generalization of (2) in terms of the ‘‘invariant’’ Stokes parameters $\mathbf{S} \equiv (I, Q, U, V) \equiv (I_\nu, Q_\nu, U_\nu, V_\nu)/v^3$ that explicitly accounts for the rotation of an observer frame along the line of sight (in our notation, the absence of subscript ν implies an invariant quantity; thus $\alpha_I \equiv v\alpha_{\nu,I}$). This generalization has been used by Broderick & Loeb (2009b), Shcherbakov et al. (2012), Gold et al. (2016), Dexter (2016), Mościbrodzka et al. (2017) to generate polarized models of accretion onto a black hole.

The covariant Stokes formulation of the polarized transfer equation is not written in manifestly covariant form, and hence the transformation of Stokes parameters from one frame to another is not completely transparent, although in the end, it amounts to a rotation. Gammie & Leung (2012) (see also Kosowsky 1996, Weinberg 2008) rewrote the polarized transport equation in terms of the rank-2, Hermitian, coherency tensor

$$N^{\alpha\beta} \equiv C \langle a_k^\alpha a_k^{*\beta} \rangle, \quad (8)$$

where a_k is a Fourier component of the four-vector potential and C is an arbitrary constant. This description is manifestly covariant.

Let us relate $N^{\alpha\beta}$ to the Stokes parameters defined in an orthonormal tetrad $e_{(a)}^\mu$ (parenthesized lowercase roman letters indicate tetrad indices). We make two assumptions about the tetrad: $e_{(t)}^\mu = u^\mu$, the four-velocity of the associated observer; and $e_{(3)}^\mu = k^\mu - \omega u^\mu$. In words: the third spatial

basis element is a unit vector oriented parallel to the spatial component of the wavevector.

It is then helpful to define four auxiliary tensors in the tetrad frame:

$$m_I \equiv \begin{pmatrix} 0 & 0 & 0 & 0 \\ 0 & 1 & 0 & 0 \\ 0 & 0 & 1 & 0 \\ 0 & 0 & 0 & 0 \end{pmatrix}, \quad (9)$$

$$m_Q \equiv \begin{pmatrix} 0 & 0 & 0 & 0 \\ 0 & 1 & 0 & 0 \\ 0 & 0 & -1 & 0 \\ 0 & 0 & 0 & 0 \end{pmatrix}, \quad (10)$$

$$m_U \equiv \begin{pmatrix} 0 & 0 & 0 & 0 \\ 0 & 0 & 1 & 0 \\ 0 & 1 & 0 & 0 \\ 0 & 0 & 0 & 0 \end{pmatrix}, \quad (11)$$

$$m_V \equiv \begin{pmatrix} 0 & 0 & 0 & 0 \\ 0 & 0 & -i & 0 \\ 0 & i & 0 & 0 \\ 0 & 0 & 0 & 0 \end{pmatrix}. \quad (12)$$

These are just the Pauli matrices (see López Ariste & Semel 1999 for a discussion) in the two dimensional space perpendicular to u^μ and the wave three-vector. Then we define C so that

$$N^{(a)(b)} = m_A^{(a)(b)} S_A \quad (13)$$

(again, the index A is one of I, Q, U, V), S_A is a component of the invariant Stokes vector \mathbf{S} , and summation over A is implied. The inverse relation is

$$S_A = \frac{1}{2} m_A^{*(a)(b)} N_{(a)(b)}. \quad (14)$$

These linear relations between N and S are easy to implement numerically. It is also obvious how N transforms under boosts, rotations, and general coordinate transformations, because it is a tensor.

The covariant polarized transport equation is

$$k^\mu \nabla_\mu N^{\alpha\beta} = J^{\alpha\beta} + H^{\alpha\beta\gamma\delta} N_{\gamma\delta}. \quad (15)$$

Here ∇_μ is a covariant derivative (the derivative operator is understood to follow a photon trajectory in frequency space), $J^{\alpha\beta}$ is an emissivity tensor, and $H^{\alpha\beta\gamma\delta}$ incorporates absorption and Faraday rotation. Expanding the covariant derivative in a coordinate basis, (15) becomes

$$\frac{dN^{\alpha\beta}}{d\lambda} = -\Gamma_{\mu\nu}^\alpha k^\mu N^{\nu\beta} - \Gamma_{\mu\nu}^\beta k^\mu N^{\alpha\nu} + J^{\alpha\beta} + H^{\alpha\beta\gamma\delta} N_{\gamma\delta}. \quad (16)$$

Here

$$J^{(a)(b)} = m_A^{(a)(b)} j_A, \quad (17)$$

and

$$H^{(a)(b)(c)(d)} = \frac{1}{2} m_A^{(a)(b)} M_{AB} m_B^{*(c)(d)}, \quad (18)$$

where M_{AB} is the matrix of absorption and rotation coefficients that appears in (6). For models in which absorption and rotation can be described in terms of the classical response of the plasma, the tensor $H^{(a)(b)(c)(d)}$ is directly related to the components of the plasma dielectric tensor; the

³ The sign of ρ_U differs from Dexter (2016) and agrees with Landi Degl’Innocenti & Landi Degl’Innocenti (1985), but this has no effect on the Dexter (2016) solution because $\rho_U = 0$ in the frame in which the transfer coefficients are evaluated.

relationship is given in [Gammie & Leung \(2012\)](#) (their eq. 64). This form of the polarized transport equation is equivalent to that used in [Broderick & Blandford \(2004\)](#).

3 NUMERICAL METHODS

Equation (16) might seem an unpromising start for a numerical integration scheme, since the basic equation is complicated and one has to integrate the 16 real degrees of freedom in $N^{\alpha\beta}$ compared to the 4 real degrees of freedom in a Stokes basis representation of the radiation field. Still, $N^{\alpha\beta}$ is manifestly covariant and conceptually simple: the tensor notation takes care of all frame transformations automatically. Also, the integration of additional degrees of freedom is, it turns out, not the leading cost in polarized ray-tracing calculations.

Our second-order integration strategy splits (16) into two parts. The first part incorporates parallel transport: it uses the LHS and the *first* two terms on the RHS to parallel transport the polarized radiation field in the coordinate basis. The second part incorporates emission, absorption, and Faraday rotation: it transforms the LHS and the *second* two terms on the RHS into the Stokes basis in the frame of the plasma, where the transfer coefficients are most naturally evaluated. These latter terms yield

$$\frac{d}{d\lambda} \begin{pmatrix} I \\ Q \\ U \\ V \end{pmatrix} = \begin{pmatrix} j_I \\ j_Q \\ j_U \\ j_V \end{pmatrix} - \begin{pmatrix} \alpha_I & \alpha_Q & \alpha_U & \alpha_V \\ \alpha_Q & \alpha_I & \rho_V & -\rho_U \\ \alpha_U & -\rho_V & \alpha_I & \rho_Q \\ \alpha_V & \rho_U & -\rho_Q & \alpha_I \end{pmatrix} \begin{pmatrix} I \\ Q \\ U \\ V \end{pmatrix} + \dots \quad (19)$$

where, again, the absence of subscript ν implies that a term appears in invariant form, i.e. $\rho_V = \nu\rho_{\nu,V}$ and the derivative is understood to follow an individual photon in frequency space.

What technique should one use to evolve (19)? One consideration is computational expense when the Faraday or absorption depth is large. Most explicit schemes will be limited by $\Delta\lambda \lesssim \text{MIN}(1/\alpha_A, 1/\rho_A)$. Many λ -steps are then required to cross the system, even if the transfer coefficients change smoothly. For example, the Faraday rotation in some models of Sgr A* and M87 at 1.3mm is very large (e.g., [Mościbrodzka et al. 2017](#)), so a simple second-order integration scheme would require many λ -steps to cross the system as it would be limited to rotating the electric vector polarization angle (EVPA) by $O(1)$ radian per step. A second consideration is that the source models that motivated the development of `ipole` are derived from numerical simulations, which have an irreducible granularity because they represent the physical variables on a grid. It makes no sense to meticulously integrate (19) across a single simulation zone when the structure of the model inside the zone is known only up to truncation error. Still, even in this case a stable and physically sensible evolution of (19) is desirable.

It would therefore be helpful to use a numerical technique that takes advantage of analytic solutions to (19) assuming constant transfer coefficients. Indeed, this is what the DELO family of polarized transfer solvers does ([Rees et al. 1989](#), [Janett et al. 2017](#)) while making particular assumptions about conditions in the source. More generally, [Landi Degl'Innocenti & Landi Degl'Innocenti \(1985\)](#) (hereafter LDI²) found an elegant, formal solution of the

problem expressed in terms of an integral along the line of sight. This solution can be also found in [Peraiah \(2001\)](#) (notice that section 12.6 contains a few typographical errors in their equations: 12.6.10, 12.6.27, 12.6.29, 12.6.31, 12.6.32) and, partially, in [Dexter \(2016\)](#) (contains a typographical error in [D5], $M_3[0,2]$ should be $\Lambda_1\alpha_U + \sigma\Lambda_2\rho_U$). Our integration scheme uses the LDI² solution in explicit form.

The explicit general polarized transport solution with constant coefficients can be obtained following LDI², who write the transfer equation (19) in the form

$$\frac{dS_A}{d\lambda} = j_A - K_{AB}S_B, \quad (20)$$

where we have recast the equation using our index notation, substituted j_A for their \mathbf{KS} (\mathbf{S} is LDI²'s source function vector), and cast the basic equation in invariant form with independent variable λ rather than s . The formal solution is

$$S_A(\lambda) = \int_{\lambda_0}^{\lambda} O_{AB}(\lambda - \lambda') j_B d\lambda' + O_{AB}(\lambda - \lambda_0) S_B(\lambda_0), \quad (21)$$

where O_{AB} is given by their eq. (10).⁴ This formal solution still requires evaluation of the integral to put it in a form suitable for numerical integration. Defining

$$P_{AB} \equiv \int_{\lambda_0}^{\lambda} O_{AB}, \quad (22)$$

the formal solution for constant coefficients is

$$S_A(\lambda) = P_{AB}(\lambda - \lambda_0) j_B + O_{AB}(\lambda - \lambda_0) S_B(\lambda_0). \quad (23)$$

Integrating LDI² eq.(10), one finds

$$\begin{aligned} P_{AB} = & -\Lambda_1 f_1 M_{3,AB} + \frac{\alpha_I f_1}{2} (M_{1,AB} + M_{4,AB}) \\ & + \Lambda_2 f_2 M_{2,AB} + \frac{\alpha_I f_2}{2} (M_{1,AB} - M_{4,AB}) \\ & - e^{-\alpha_I \Delta\lambda} \times \\ & \left\{ \left[-\Lambda_1 f_1 M_{3,AB} + \frac{\alpha_I f_1}{2} (M_{1,AB} + M_{4,AB}) \right] \cosh(\Lambda_1 \Delta\lambda) \right. \\ & + \left[-\Lambda_2 f_2 M_{2,AB} + \frac{\alpha_I f_2}{2} (M_{1,AB} - M_{4,AB}) \right] \cos(\Lambda_2 \Delta\lambda) \\ & + \left[-\alpha_I f_2 M_{2,AB} - \frac{\Lambda_2 f_2}{2} (M_{1,AB} - M_{4,AB}) \right] \sin(\Lambda_2 \Delta\lambda) \\ & \left. - \left[\alpha_1 f_1 M_{3,AB} - \frac{\Lambda_1 f_1}{2} (M_{1,AB} + M_{4,AB}) \right] \sinh(\Lambda_1 \Delta\lambda) \right\}. \quad (24) \end{aligned}$$

Here $\Delta\lambda \equiv \lambda - \lambda_0$ and the notation follows LDI² including the definition of the 4×4 matrices M , except that we have introduced $f_1 \equiv (\alpha_I^2 - \Lambda_1^2)^{-1}$ and $f_2 \equiv (\alpha_I^2 + \Lambda_2^2)^{-1}$, and our α_S is their η_S . The reader is referred to LDI², or the publicly released code, for a complete account of the solution.

Solution (23) is complicated and difficult to manipulate algebraically. For convenience, we provide two special solutions in the appendix, for when only Faraday conversion is present and for when only absorption and emission are present.

⁴ There is a typographical error in $M_4[1, 1]$; n_Q should read η_Q .

3.1 Integration scheme

The full image-generation routine proceeds as follows. The basic notion is identical to the publicly available `ibothros` code.⁵ An observer is placed at a fixed spacetime event and given a four-velocity and a “camera” which is defined via an orthonormal tetrad at the observer. The camera has pixels, which form a regular grid in angle. If the camera is pointed at the black hole, the central point of the frame is defined so that photons arriving at that point have zero angular momentum. Geodesics are integrated backwards from the center of each pixel through the source until a stopping condition is met (the stopping condition is problem dependent). The coordinates and wavevectors along the geodesic are recorded during the backwards integration.

The transfer equation is then integrated *forward* along the geodesic to the camera. Begin by setting the Stokes vector using a boundary condition, usually $S_A = 0$. Then convert S_A to $N^{\alpha\beta}$ using 13 and evolve $N^{\alpha\beta}$ forward along the geodesic.

(1) Evaluate the connection coefficient at the initial position and parallel transport $N^{\alpha\beta}$ by a half step using the first two terms in (16). This is done using a simple second-order integrator. Since the rest of the scheme is second order there is no point in going to higher order.

(2) Erect an orthonormal tetrad $e_{(a)}^\mu$ in the plasma frame at the half-step position, with $e_{(0)}^\mu = u^\mu$, the plasma four-velocity, $e_{(3)}^\mu$ parallel to the spatial component of the wavevector in the plasma frame, and $e_{(1)}^\mu$ and $e_{(2)}^\mu$ in the plane perpendicular to both. In most problems of interest to us synchrotron emission is important, so ordinarily we require that $e_{(2)}$ is in the plane formed by the wavevector and the magnetic field in the plasma frame. Adopt the convention that $Q > 0$ corresponds to linear polarization in the $e_{(1)}$ direction. Then for synchrotron emission and absorption, $j_U = \alpha_U = 0$, and if Faraday conversion is due to a magnetized plasma then $\rho_U = 0$.

(3) Evaluate the transfer coefficients in the tetrad frame.

(4) Project $N^{\alpha\beta}$ into S_A in the tetrad frame.

(5) Evolve the Stokes vector by a full λ step using the analytic solution (23).

(6) Transform S_A back into $N^{\alpha\beta}$ using the tetrad basis.

(7) Parallel transport $N^{\alpha\beta}$ by another half-step.

Substeps (7) and (1) can be combined without formal loss of accuracy if a half-step is taken at the beginning and end of the integration and the stepsize is constant. The initial and final half-step can also be dropped without loss of accuracy if they occur in regions where there is no substantial evolution of $N^{\alpha\beta}$.

Finally, the Stokes parameters are observed in the camera tetrad using equation (14) and recorded at each pixel.

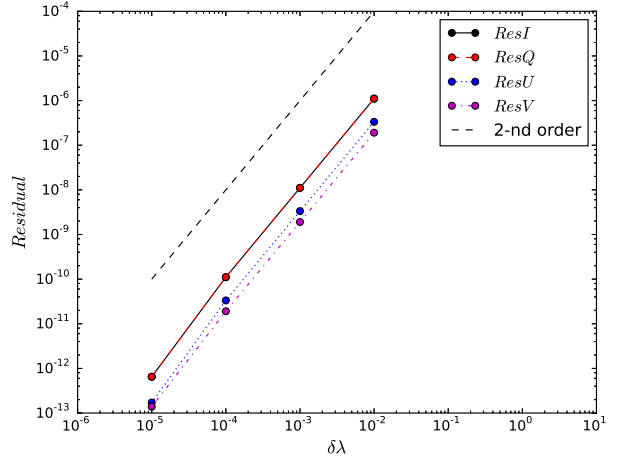


Figure 1. Transport-step test no 1: Convergence of the transport-step in vacuum when polarized light is transported in Minkowski space with “snake” Cartesian coordinates. The residuals between the Stokes parameters at the beginning and at the end of integration path are shown as a function of the step-size. The transport scheme converges at second order.

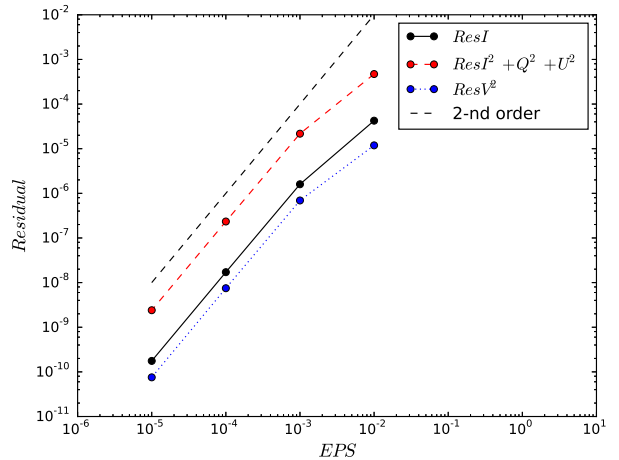


Figure 2. Transport-step test no 2: Convergence of the transport-step in vacuum in a near vicinity of the event horizon of the Kerr black hole. Here we show residuals of invariant quantities between initial and final integration point as a function of parameter describing the step-size. The transport scheme converges at second order.

4 TESTS OF NUMERICAL SCHEME

4.1 Tests of transport step in non-trivial geometries

The parallel transport of k^μ and $N^{\alpha\beta}$ is realized using a second-order integrator (meaning the single-step error is

⁵ <https://github.com/AFD-Illinois/ibothros2d>

$O(\Delta\lambda^3)$ and therefore the error at the camera is $O(\Delta\lambda^2)$ after integrating over $O(\Delta\lambda^{-1})$ steps). Parallel transport tests considered in this section assume a non-zero initial $N^{\alpha\beta}$ and transport $N^{\alpha\beta}$ in vacuum (i.e. we are solving (16) assuming that all transport coefficients vanish). We test the transport of polarized light in i) Minkowski spacetime using snake Cartesian coordinates (see section 4.3 in White et al. 2016) and ii) Kerr spacetime described by modified Kerr-Schild coordinates (Gammie et al. 2003).

i) The snake coordinates (X^0, X^1, X^2, X^3) vary periodically with Minkowski position (t, x, y, z) . The two coordinate systems are related via $(X^0, X^1, X^2, X^3) = (t, x, y + a \sin(kx), z)$, where $a = 0.3$ and $k = \pi/2$ are default parameters. For $\delta = ak \sin(kX^1)$ the geometry is described by the following metric tensor:

$$g_{\mu\nu} = \begin{pmatrix} -1 & 0 & 0 & 0 \\ 0 & \sqrt{1+\delta^2} & -\delta & 0 \\ 0 & -\delta & 1 & 0 \\ 0 & 0 & 0 & 1 \end{pmatrix}. \quad (25)$$

In snake coordinates (16) has source terms because the connection coefficient Γ_{11}^2 does not vanish. We find Γ_{11}^2 by numerically differentiating the metric tensor (a facility for obtaining the connection coefficients by numerical differentiation of the metric is provided in the default, public version of the code).

In flat spacetime, in the absence of emitting and absorbing matter, the Stokes parameters should remain constant when measured in a parallel transported tetrad attached to k^μ (here Q and U are read out in a tetrad in which the basis vectors perpendicular to k^μ are aligned with the snake coordinates). Figure 1 displays residuals of Stokes parameters extracted from $N^{\alpha\beta}$ at $x_{\text{final}} = 3$ (where x_{final} is the end of the integration path that starts at $x_{\text{init}} = 0$) with respect to their initial values as a function of the constant step size. As expected, the residuals decrease as $(\Delta\lambda)^2$.

ii) In the second test we check performance of the parallel transport in Kerr metric in modified Kerr-Schild coordinates. Here the integration is carried out along geodesics that pass the black hole event horizon with an impact parameter of $5 GM/c^2$. The black hole dimensionless angular momentum parameter $a/M = 0.9375$. First, we checked that during integration the parallel transported rank-2 tensor $N^{\alpha\beta}$ remains Hermitian. Second, we check three invariant quantities along the ray: Stokes I , combination of Stokes parameters $I^2 + Q^2 + U^2$, and V^2 . Figure 2 shows residuals between initial invariant quantities and the ones measured at the end of geodesics integration (at large distance from the black hole). The residuals are shown as a function of step-size control parameter EPS . The residuals evidently decrease as EPS^2 . Our second order scheme has single precision accuracy for $\text{EPS} \lesssim 10^{-3}$, which is the value we typically use in `ibothros` when generating mock observations of a GRMHD simulation.

Figure 2 demonstrates the convergence of the transport scheme in Kerr metric along a single geodesic. We are interested in constructing images of an accreting black hole at a camera located far from the hole. In the third test we demonstrate the accuracy of the transport step when constructing such images. The observer is located at $r_{\text{cam}} = 10^6 GM/c^2$. The observer's line of sight is oriented at 90 degrees with respect to the black hole spin axis. We set a screen pro-

ducing a uniformly polarized radiation at $r = 10^4 GM/c^2$ behind the black hole. The screen has size $10^4 \times 10^4 GM/c^2$. The Stokes parameters at the screen are generated using the same tetrad construction procedure as that used for the camera. A checkerboard pattern in Stokes I is introduced to help visualize how gravitational lensing distorts the background screen. The degree of linear polarization $LP = \sqrt{Q^2 + U^2}/I = 100$ per cent and degree of circular polarization $CP = |V|/I = 25$ per cent are constant across the entire screen.

Figure 3 shows how a Kerr black hole distorts the background checkerboard pattern. Top and bottom panels show the same model at large and small scales, respectively. For a large field-of-view the pattern is only weakly affected by the gravitational field of the black hole. For a smaller field-of-view the pattern is strongly lensed and the image of the screen edges resemble a four-leaf clover. In vacuum Stokes I, $I^2 + Q^2 + U^2$ and V^2 are invariant, and consequently the linear and circular polarization fractions are invariant. We find that these radiative transport invariants are conserved for any given ray that reaches the observer with accuracy better than 0.01 percent. Notice however that the polarization angle $EVPA$ is a function of ray impact parameter. The $EVPA$ rotation is expected because of gravitational Faraday rotation (e.g., Ishihara et al. 1988, Sereno 2005).

4.2 Tests source step combined with transport step

Next we test the part of the code that evolves the Stokes parameters. Dexter (2016) (Appendix C) presents two cases where (6) has an analytic solution in a simple functional form. These two examples are in Minkowski spacetime and either $j_{IQ} \neq 0$ and $\alpha_{IQ} \neq 0$ or $j_{QUV} \neq 0$ and $\rho_{QV} \neq 0$. Other transfer coefficients are set to zero. Here we repeat these two tests in the snake coordinates.

In the first test, $j_{IQ} = (2, 1)$ and $\alpha_{IQ} = (1, 1.2)$ are the only non-zero elements on the RHS of (16) (apart from the Γ_{11}^2 coefficient needed for parallel transport in snake coordinates). Figure 4 (left panel) compares the `ipole` numerical and known analytic solutions. For step size $\Delta\lambda = 10^{-3}$ (although for constant transfer coefficients our errors do not depend on the step size) the residuals between numerical and analytic model are better than single-precision accuracy.

In the second test, $j_{QUV} = (0.1, 0.1, 0.1)$ and $\rho_{QV} = (10, -4)$. Figure 4 (right panel) shows the results. Here, the residuals between numerical and analytic solution are even smaller compared to the emission/absorption test in the left panel. The errors oscillate and grow with λ .

4.3 Comparison of `ipole` and `grtrans`

4.3.1 Relativistic plasma in Minkowski space

Next, we consider a radiative transfer problem in a slab of relativistically hot, magnetized plasma with varying plasma density, temperature, magnetic field strength and magnetic field direction. The plasma is emitting, absorbing, and Faraday rotating/converting polarized synchrotron radiation. This problem has no analytic solution, so we test by comparison with `grtrans`.

We use the same j_S , α_S and ρ_S as those in `grtrans`. The

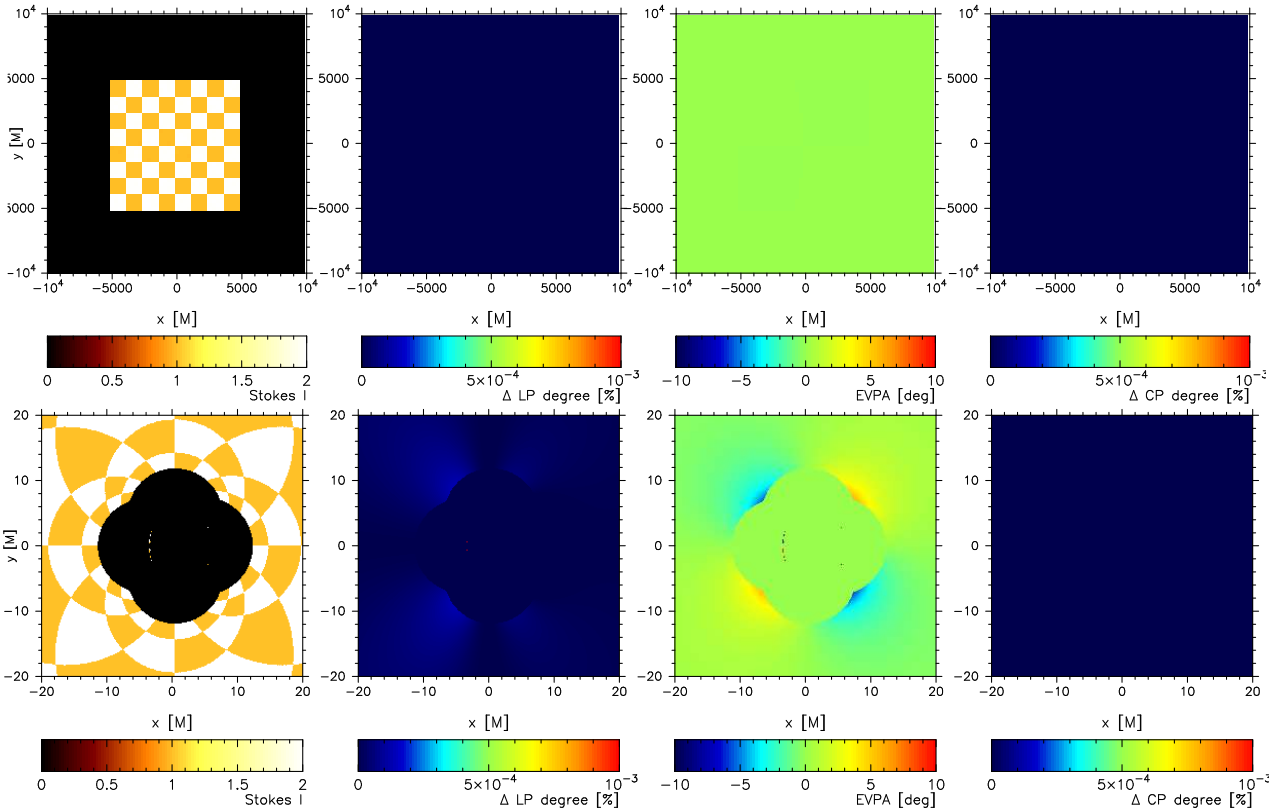


Figure 3. Transport-step test no 3: image of uniformly polarized screen (of size equal $10^4 \times 10^4$ M) behind the spinning black hole. Observer’s viewing angle is 90 degrees with respect to the black hole spin axis. The upper panels show the image of the screen for a large field-of-view to show the problem setup. At these scales the image is barely affected by the gravitational lensing and EVPA is zero. The lower panels show the zoom-in of the upper panels onto inner regions where lensing is significant and therefore distorts the checkerboard pattern. Panels from left to right show: Stokes I (transport-step invariant), the change of linear polarization degree (transport-step invariant), EVPA and the change of circular polarization degree (which square value is also the transport-step invariant). Here we see some rotation of polarization angle.

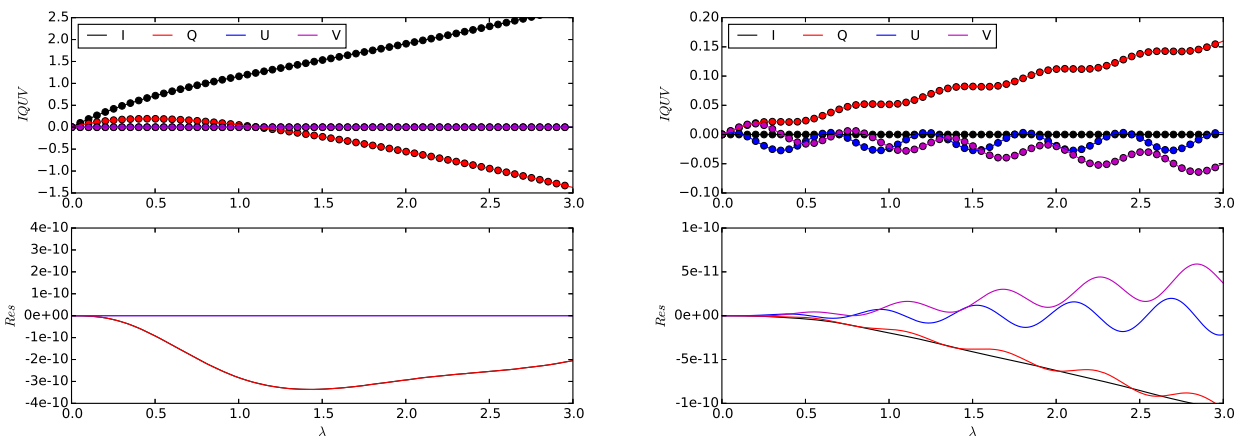


Figure 4. Source-step tests no 1 and 2: Numerical (points) and analytic (lines) solutions of radiative transport of polarized light in 1D in snake coordinates. Left panel: test of emission and absorption of Stokes I and Q . Right panel: test of emission and rotation of Stokes Q , U , and V (see text for details).

exact formulae for emissivity, absorptivity, and rotativity are written down in Dexter (2016) in appendices A1 and B2. The expressions for Faraday rotativities follow Shcherbakov (2008). Each coefficient is a distinct function of plasma density, temperature, magnetic field strength, photon frequency, and orientation of the magnetic field with respect to k^μ . This test also allows us to test our implementations of units, as both codes produce results in cgs units.

We integrate (16) along the x -axis from $x = -15L$ to $x = 15L$, where $L = 10^{15}$ cm. The plasma electron number density varies smoothly with x as

$$n_e = n_0 \left[1 + A \exp^{-(x/L)^2/\sigma_x^2} \right], \quad (26)$$

where $n_0 = 10^2$, $A = 10^4$, and $\sigma_x = 4$ are free parameters. The electrons have a relativistic, thermal (Maxwell-Jüttner) distribution function described by dimensionless electron temperature $\Theta_e = k_B T_e / (m_e c^2)$. Electron temperature is also a smooth, slowly changing function of x :

$$\Theta_e = \Theta_{e,0} \left[1 + A \exp^{-(x/L)^2/\sigma_x^2} \right], \quad (27)$$

where $\Theta_{e,0} = 20$, $A = -0.99$, and $\sigma_x = 10$ are free parameters. The density and temperature profiles are shown in Figure 5 (top left panel). For simplicity, we assume that magnetic field strength $B=30$ Gauss and its orientation $\theta = 60$ degrees are constant along the integration path. Also the spatial components of the plasma four-velocity are zero. The radiative transfer equations are integrated for a photon with frequency of 230 GHz. The invariant synchrotron emissivities, absorptivities, and rotativities and their ratios along the integration path are shown in Figure 5. Two bottom panels in Figure 5 show the optical and Faraday optical thickness per integration step.

Figure 6 shows radiative transfer solutions through the plasma shown in Figure 5. Here all Stokes parameters are shown in cgs units as produced by `ipole` and `grtrans`. The codes agree with each other well, except for Stokes Q and U in regions with high Faraday depth (between $x = -3L$ and $x = 5L$) where Q, U and V are small.

4.3.2 Polarized transport in hot accretion flows onto a black hole

In Figure 7 (upper panels) we present an example of `ipole` polarized images of hot, magnetized turbulent accretion flow around a Kerr black hole. The underlying plasma accretion flow model is a 3D GRMHD Fishbone-Moncrief torus simulation carried out with `harm3d` code (Gammie et al. 2003, Noble et al. 2006). The simulation data is converted from the code units to cgs units assuming black hole mass $M_{\text{BH}} = 6.2 \times 10^9 M_\odot$ and the mass accretion rate onto the black hole $\dot{M} = 1.1 \times 10^{-4} M_\odot \text{yr}^{-1}$. The model requires a prescription for electron temperature; we assume that electron temperature equals proton temperatures in the entire computational domain. In this test, the observer is located at distance of $r=1000 M$ from the black hole and the line of sight is at 60 degrees to the black hole spin axis.

We repeat the radiative transport calculation through the same simulation snapshot using `grtrans`. Figure 7 (lower panels) shows difference between `ipole` and `grtrans` outputs. The differences are small. We quantify the difference between images using mean square error defined as

$MSE_S = \sum_{ij} (S_{\text{ipole}} - S_{\text{grtrans}})^2 / \sum_{ij} S_{\text{grtrans}}^2$, where S is the Stokes parameter and summations are done over all image pixels. The results are $MSE_I = 4.38 \times 10^{-5}$, $MSE_Q = 1.44 \times 10^{-3}$, $MSE_U = 9 \times 10^{-4}$, and $MSE_V = 3.92 \times 10^{-3}$ for stepping parameter $\text{EPS} = 0.0025$. One can also quantify the agreement between two corresponding Stokes maps using the image quality index Q_{idx} (Wang & Bovik 2002). We find $Q_{\text{idx}}(I, Q, U, V) = (0.999968, 0.999173, 0.998880, 0.995589)$, where $Q_{\text{idx}}=1$ would mean that two images are identical, which confirms strong consistency between corresponding Stokes maps. We conclude that the agreement between the two codes is excellent even for a very complex problems.

In the future we will test the convergence of radiative transfer simulations through various GRMHD simulations as a function of the step size along geodesics and as a function of number of pixels in the images. In our example calculation we also assumed that the dynamical simulations are static and the plasma conditions do not change as the light propagates through it (the ‘‘fast light’’ approximation). Near a black hole event horizon, however, the light crossing time is comparable to the dynamical time. It is important to quantify how sensitive the observed Stokes parameters are to spatial and temporal resolution (i.e., cadences of data dumps) of the numerical simulations, but such a study is beyond the scope of the present paper.

5 SUMMARY

We have designed a numerical scheme capable of integrating relativistic polarized radiative transfer equations by ray tracing in non-trivial spacetimes and in optical and Faraday thick plasmas. We have demonstrated that the integration scheme is stable and accurate and can reproduce known analytic solutions. The code has been tested on scaled problems and on dimensional problems to test the unit system. Our results agree with results from J. Dexter’s independent code, `grtrans`.

We plan to extend `ipole` to include scattering within a Monte Carlo framework, so that it can make predictions for a broader range of sources and photon energies (Connors & Stark 1977, Connors et al. 1980), motivated by results from INTEGRAL and the future X-ray polarization mission IXPE.

Does the code run efficiently, i.e. how fast is it? Our reference machine is a two socket Intel Xeon E5-2660 at 2.6 GHz, which has a total of 20 physical cores (40 with hyperthreading). We compile the code with a version of `h5cc` that uses `gcc 4.8.5` and `-Ofast -fopenmp`. We find that a 256^2 fully polarized image with a $40GM/c^2$ field of view, using data from a `harm3d` model, completes in 8.6s clocktime and 253s cpu time. On a single core, the code completes in 136s, for an average speed of 480 rays per second. This speed is similar to that of `ibothros2d`.

`ipole` is publicly available at <https://github.com/moscibrodzka/ipole> (note: the code will be released simultaneously with publication).

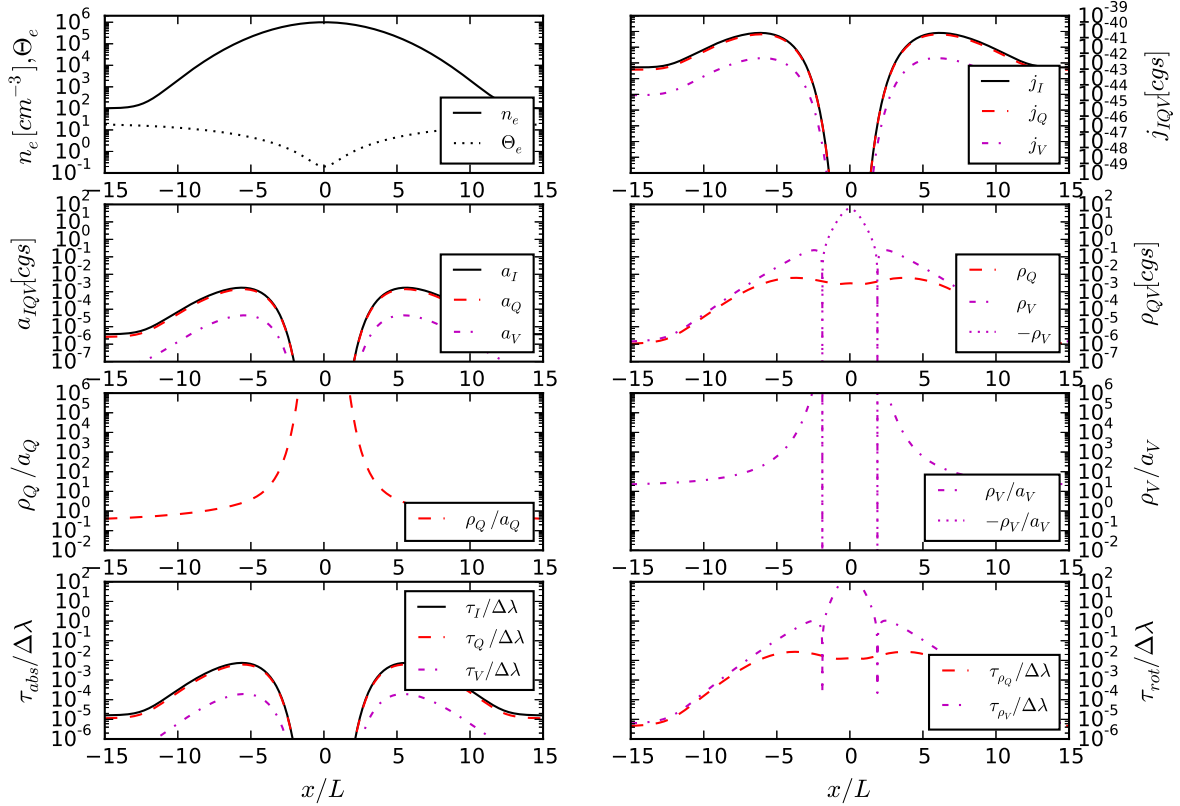


Figure 5. Source-step test no 3: structure of the slab of plasma together with all synchrotron emissivities, absorptivities and rotativities, their ratios and optical and Faraday thickness per one step along the integration path.

ACKNOWLEDGEMENTS

M. Mościbrodzka acknowledges support from the ERC Synergy Grant “BlackHoleCam-Imaging the Event Horizon of Black Holes” (Grant 610058). C. F. Gammie acknowledges support from NSF grant AST-1333612 and AST-1716327, a Romano Professorial Scholarship, and the hospitality of the Flatiron Institute’s Center for Computational Astrophysics where some of this work was completed. The authors thank J. Dexter for his extensive help and guidance. The authors also thank B. Ryan, G. Janett, and the referee for their comments.

REFERENCES

- Balazs N. L., 1958, *ApJ*, **128**, 398
 Ball D., Özel F., Psaltis D., Chan C.-k., 2016, *ApJ*, **826**, 77
 Bower G. C., Wright M. C. H., Falcke H., Backer D. C., 2003, *ApJ*, **588**, 331
 Bower G. C., Falcke H., Wright M. C., Backer D. C., 2005, *ApJ*, **618**, L29
 Broderick A., Blandford R., 2004, *MNRAS*, **349**, 994
 Broderick A. E., Loeb A., 2005, *MNRAS*, **363**, 353
 Broderick A. E., Loeb A., 2009a, *ApJ*, **697**, 1164
 Broderick A. E., Loeb A., 2009b, *ApJ*, **697**, 1164
 Broderick A. E., Fish V. L., Doeleman S. S., Loeb A., 2009, *ApJ*, **697**, 45
 Broderick A. E., Fish V. L., Doeleman S. S., Loeb A., 2011a, *ApJ*, **735**, 110
 Broderick A. E., Fish V. L., Doeleman S. S., Loeb A., 2011b, *ApJ*, **738**, 38
 Bromley B. C., Melia F., Liu S., 2001, *ApJ*, **555**, L83
 Chan C.-k., Psaltis D., Özel F., 2013, *ApJ*, **777**, 13
 Chan C.-K., Psaltis D., Özel F., Narayan R., Sadowski A., 2015, *ApJ*, **799**, 1
 Chan C.-k., Medeiros L., Ozel F., Psaltis D., 2017, preprint, ([arXiv:1706.07062](https://arxiv.org/abs/1706.07062))
 Connors P. A., Stark R. F., 1977, *Nature*, **269**, 128
 Connors P. A., Stark R. F., Piran T., 1980, *ApJ*, **235**, 224
 Cunningham C. T., 1975, *ApJ*, **202**, 788
 Cunningham C. T., Bardeen J. M., 1973, *ApJ*, **183**, 237
 Dexter J., 2016, *MNRAS*, **462**, 115
 Dexter J., Agol E., 2009, *ApJ*, **696**, 1616
 Dexter J., Fragile P. C., 2011, *ApJ*, **730**, 36
 Dexter J., Fragile P. C., 2013, *MNRAS*, **432**, 2252
 Dexter J., Agol E., Fragile P. C., McKinney J. C., 2010, *ApJ*, **717**, 1092
 Dexter J., McKinney J. C., Agol E., 2012, *MNRAS*, **421**, 1517
 Dolence J. C., Gammie C. F., Shiokawa H., Noble S. C., 2012, *ApJ*, **746**, L10
 Eckart A., et al., 2008, *A&A*, **479**, 625
 Falcke H., Melia F., Agol E., 2000, *ApJ*, **528**, L13
 Fraga-Encinas R., Mościbrodzka M., Brinkerink C., Falcke H., 2016, *A&A*, **588**, A57
 Gammie C. F., Leung P. K., 2012, *ApJ*, **752**, 123

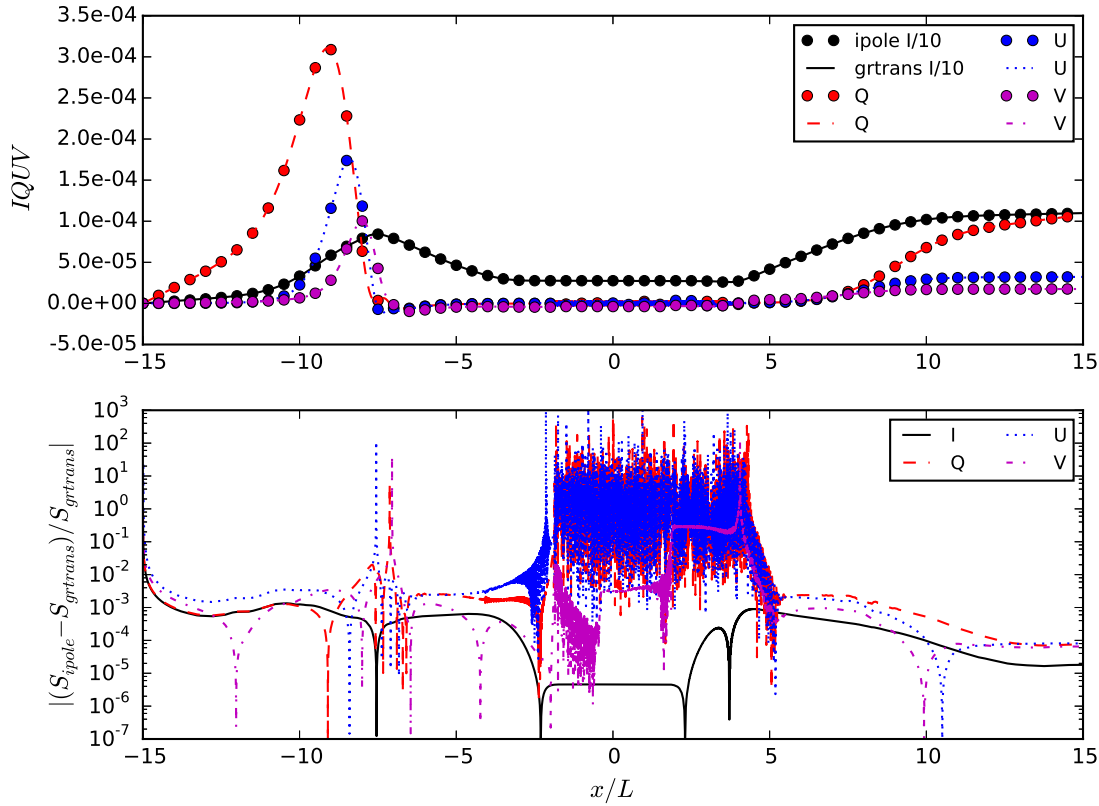


Figure 6. Source-step test no 3: Comparison of radiative transfer integration with `ipole` and `grtrans` schemes. The largest difference is in Stokes Q , U , and V in regions of large Faraday optical depth, $\tau_F \gg 1$. Otherwise the relative difference between the codes is less than 1%.

- Gammie C. F., McKinney J. C., Tóth G., 2003, *ApJ*, **589**, 444
- Gold R., McKinney J. C., Johnson M. D., Doeleman S. S., 2016, preprint, ([arXiv:1601.05550](https://arxiv.org/abs/1601.05550))
- Hamaker J. P., Bregman J. D., 1996, *A&AS*, **117**, 161
- Huang L., Liu S., Shen Z.-Q., Cai M. J., Li H., Fryer C. L., 2008, *ApJ*, **676**, L119
- Ishihara H., Takahashi M., Tomimatsu A., 1988, *Phys. Rev. D*, **38**, 472
- Janett G., Carlin E. S., Steiner O., Belluzzi L., 2017, *ApJ*, **840**, 107
- Johnson M. D., et al., 2015, *Science*, **350**, 1242
- Kosowsky A., 1996, *Annals of Physics*, **246**, 49
- Kuo C. Y., et al., 2014, *ApJ*, **783**, L33
- Landi Degl'Innocenti E., Landi Degl'Innocenti M., 1985, *Sol. Phys.*, **97**, 239
- López Ariste A., Semel M., 1999, *A&A*, **350**, 1089
- Mao S. A., Dexter J., Quataert E., 2017, *MNRAS*, **466**, 4307
- Marrone D. P., Moran J. M., Zhao J.-H., Rao R., 2007, *ApJ*, **654**, L57
- Marrone D. P., et al., 2008, *ApJ*, **682**, 373
- Medeiros L., Chan C.-k., Özel F., Psaltis D., Kim J., Marrone D. P., Sadowski A., 2017, *ApJ*, **844**, 35
- Mościbrodzka M., Gammie C. F., Dolence J. C., Shiokawa H., Leung P. K., 2009, *ApJ*, **706**, 497
- Mościbrodzka M., Shiokawa H., Gammie C. F., Dolence J. C., 2012, *ApJ*, **752**, L1
- Mościbrodzka M., Falcke H., Shiokawa H., Gammie C. F., 2014, *A&A*, **570**, A7
- Mościbrodzka M., Falcke H., Shiokawa H., 2016, *A&A*, **586**, A38
- Mościbrodzka M., Dexter J., Davelaar J., Falcke H., 2017, *MNRAS*, **468**, 2214
- Muñoz D., Marrone D., Moran J., 2009, in American Astronomical Society Meeting Abstracts #214. p. 761
- Muñoz D. J., Marrone D. P., Moran J. M., Rao R., 2012, *ApJ*, **745**, 115
- Noble S. C., Gammie C. F., McKinney J. C., Del Zanna L., 2006, *ApJ*, **641**, 626
- Noble S. C., Leung P. K., Gammie C. F., Book L. G., 2007, *Classical and Quantum Gravity*, **24**, S259
- Peraiah A., 2001, *An Introduction to Radiative Transfer*. Cambridge University Press
- Porth O., Olivares H., Mizuno Y., Younsi Z., Rezzolla L., Mościbrodzka M., Falcke H., Kramer M., 2017, *Computational Astrophysics and Cosmology*, **4**, 1
- Pu H.-Y., Yun K., Younsi Z., Yoon S.-J., 2016a, *ApJ*, **820**, 105
- Pu H.-Y., Akiyama K., Asada K., 2016b, *ApJ*, **831**, 4
- Rees D. E., Durrant C. J., Murphy G. A., 1989, *ApJ*, **339**, 1093
- Roelofs F., Johnson M. D., Shiokawa H., Doeleman S. S., Falcke H., 2017, preprint, ([arXiv:1708.01056](https://arxiv.org/abs/1708.01056))
- Sereno M., 2005, *MNRAS*, **356**, 381
- Shahzamanian B., et al., 2015, *A&A*, **576**, A20
- Shcherbakov R. V., 2008, *ApJ*, **688**, 695
- Shcherbakov R. V., Penna R. F., McKinney J. C., 2012, *ApJ*, **755**, 133

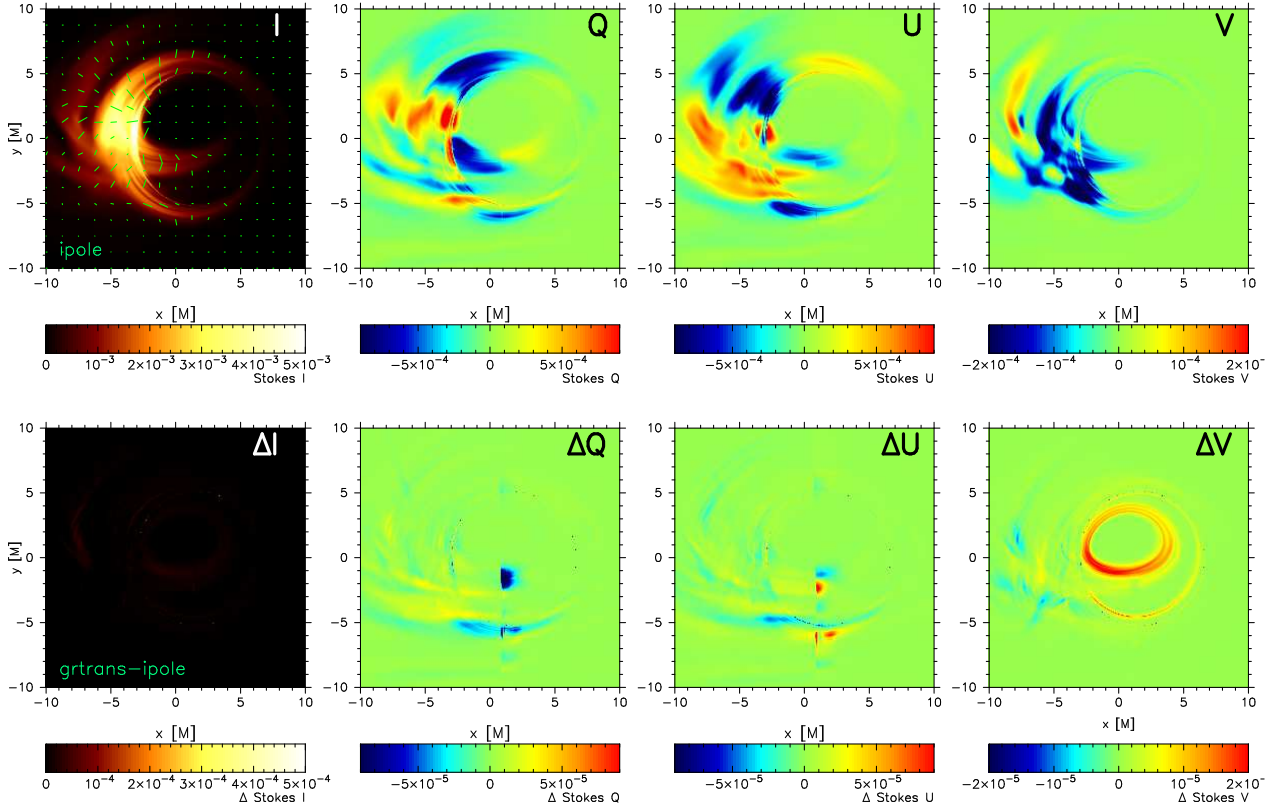


Figure 7. Polarized millimetre images of a Kerr black hole ($a/M = 0.9375$) accreting matter. The dynamics of magnetized plasma around the black hole is a 3D GRMHD model of thick accretion disk with turbulent magnetic fields. Top panels show the Stokes I (with green ticks indicating the direction of EVPA and the length of each tick being proportional to a local $\sqrt{Q^2 + U^2}$), Stokes Q, U and V. The dark circular shadow in the Stokes I map is the shadow of the black hole event horizon. Bottom panels show corresponding residuals between Stokes parameters in *ipole* and *grtrans* output. The field of view in all images is $20 \times 20 GM/c^2$ with resolution of 256×256 pixels and the observer’s line of sight is 60 degrees away from the black hole spin axis.

Shiokawa H., Gammie C. F., Doeleman S. S., 2017, preprint, ([arXiv:1708.02577](https://arxiv.org/abs/1708.02577))

Vincent F. H., Paumard T., Gourgoulhon E., Perrin G., 2011, *Classical and Quantum Gravity*, **28**, 225011

Vincent F. H., Yan W., Straub O., Zdziarski A. A., Abramowicz M. A., 2015, *A&A*, **574**, A48

Wang Z., Bovik A. C., 2002, *IEEE Signal Processing Letters*, **9**, 81

Weinberg S., 2008, *Cosmology*. Oxford University Press

White C. J., Stone J. M., Gammie C. F., 2016, *ApJS*, **225**, 22

Younsi Z., Wu K., 2015, *MNRAS*, **454**, 3283

Younsi Z., Wu K., Fuerst S. V., 2012, *A&A*, **545**, A13

Yuan Y.-F., Cao X., Huang L., Shen Z.-Q., 2009, *ApJ*, **699**, 722

van Ballegoijen A. A., 1985, in Hagyard M. J., ed., *Measurements of Solar Vector Magnetic Fields*.

APPENDIX A: SPECIAL SOLUTIONS TO POLARIZED TRANSFER EQUATION

It may be useful for tests to have simplified analytic solutions to the polarized transfer equation (19) in special cases. Here we consider solutions with Faraday rotation alone (and no absorption and emission), and when Faraday rotation is absent.

A1 Solution with Faraday rotation alone

Consider (19) with the only the rotation coefficients nonzero:

$$\frac{d}{d\lambda} \begin{pmatrix} I \\ Q \\ U \\ V \end{pmatrix} = - \begin{pmatrix} 0 & 0 & 0 & 0 \\ 0 & 0 & \rho_V & -\rho_U \\ 0 & -\rho_V & 0 & \rho_Q \\ 0 & \rho_U & -\rho_Q & 0 \end{pmatrix} \begin{pmatrix} I \\ Q \\ U \\ V \end{pmatrix}. \quad (\text{A1})$$

This can be integrated directly to find the analytic solution:

$$I = I_0 \quad (\text{A2})$$

$$Q = Q_0 \cos(\rho\lambda) + 2 \frac{\rho_Q(\rho \cdot \mathbf{S})}{\rho^2} \sin^2(\rho\lambda/2) + \frac{\rho_U V_0 - \rho_V U_0}{\rho} \sin(\rho\lambda), \quad (\text{A3})$$

$$U = U_0 \cos(\rho\lambda) + 2 \frac{\rho_U(\rho \cdot \mathbf{S})}{\rho^2} \sin^2(\rho\lambda/2) + \frac{\rho_V Q_0 - \rho_Q V_0}{\rho} \sin(\rho\lambda), \quad (\text{A4})$$

$$V = V_0 \cos(\rho\lambda) + 2 \frac{\rho_V(\rho \cdot \mathbf{S})}{\rho^2} \sin^2(\rho\lambda/2) + \frac{\rho_Q U_0 - \rho_U Q_0}{\rho} \sin(\rho\lambda), \quad (\text{A5})$$

which has a pleasing symmetry to it. Here $\rho^2 \equiv \rho_Q^2 + \rho_U^2 + \rho_V^2$, and $\rho \cdot \mathbf{S} \equiv \rho_Q Q_0 + \rho_U U_0 + \rho_V V_0$.

A2 Solution with emission and absorption alone

Now consider the piece of (19) with $\rho_A \rightarrow 0$:

$$\frac{d}{d\lambda} \begin{pmatrix} I \\ Q \\ U \\ V \end{pmatrix} = \begin{pmatrix} j_I \\ j_Q \\ j_U \\ j_V \end{pmatrix} - \begin{pmatrix} \alpha_I & \alpha_Q & \alpha_U & \alpha_V \\ \alpha_Q & \alpha_I & 0 & 0 \\ \alpha_U & 0 & \alpha_I & 0 \\ \alpha_V & 0 & 0 & \alpha_I \end{pmatrix} \begin{pmatrix} I \\ Q \\ U \\ V \end{pmatrix}. \quad (\text{A6})$$

The matrix \mathbf{M} on the RHS is real and symmetric, so one can solve by finding the eigenvalues and eigenvectors of \mathbf{M} , projecting the initial state and emission coefficients into the eigenbasis, where (19) reduces to the same form as the unpolarized radiative transfer equation, and reassembling the result in the Stokes basis.

Rather than simply stating the result, it may be helpful to give a few intermediate results. Here is an orthonormal eigenbasis for \mathbf{M} (in the Stokes basis):

$$e_1 = \frac{1}{N_1} \{0, -\alpha_V n_U, -\alpha_V n_Q, \alpha_U n_Q + \alpha_Q n_U\}, \quad (\text{A7})$$

with eigenvalue $1/\lambda_1 = \alpha_I$, $N_1 \equiv (2(\alpha_Q \alpha_U n_Q n_U + n_Q^2 n_U^2))^{1/2}$, $n_Q \equiv (\alpha_Q^2 + \alpha_V^2)^{1/2}$, $n_U \equiv (\alpha_U^2 + \alpha_V^2)^{1/2}$,

$$e_2 = \frac{1}{N_2} \{0, \alpha_V n_U, -\alpha_V n_Q, \alpha_U n_Q - \alpha_Q n_U\}/N_2, \quad (\text{A8})$$

with eigenvalue $1/\lambda_2 = \alpha_I$, $N_2 \equiv (2(-\alpha_Q \alpha_U n_Q n_U + n_Q^2 n_U^2))^{1/2}$,

$$e_3 = \frac{1}{\sqrt{2}\alpha_P} \{\alpha_P, \alpha_Q, \alpha_U, \alpha_V\}, \quad (\text{A9})$$

with eigenvalue $1/\lambda_3 = \alpha_I + \alpha_P$, $\alpha_P \equiv (\alpha_Q^2 + \alpha_U^2 + \alpha_V^2)^{1/2}$,

$$e_4 = \frac{1}{\sqrt{2}\alpha_P} \{-\alpha_P, \alpha_Q, \alpha_U, \alpha_V\}, \quad (\text{A10})$$

with eigenvalue $1/\lambda_4 = \alpha_I - \alpha_P$. Evidently if I is to decay under absorption we must have $\alpha_I \geq \alpha_P$. Notice that $1/\lambda_i$ is an eigenvalue, and λ is the affine parameter.

Finding the combined absorption and emission solution is now easy. Let $a_i(\lambda)$ be the solution for the amplitude of eigenvector e_i . The transfer equation in the eigenbasis, excluding Faraday conversion, is

$$\frac{da_i}{d\lambda} = j_i - \frac{a_i}{\lambda_i} \quad (\text{A11})$$

where $j_i = j_A e_{i,A}$. The solution is identical to the formal solution of the unpolarized transfer equation:

$$a_i(\lambda) = j_i \lambda_i (1 - e^{-\lambda/\lambda_i}) + a_i^0 e^{-\lambda/\lambda_i}. \quad (\text{A12})$$

Here a_i^0 is the initial Stokes vector projected into the eigenbasis. The solution in the Stokes basis is then

$$S_A(\lambda) = a_i(\lambda) e_{i,A}. \quad (\text{A13})$$

The final result can be written:

$$I = \left(I_0 \cosh(\alpha_P \lambda) - \frac{\alpha \cdot \mathbf{S}}{\alpha_P} \sinh(\alpha_P \lambda) \right) e^{-\alpha_I \lambda} + \frac{\alpha \cdot j}{\alpha_I^2 - \alpha_P^2} \left(-1 + \frac{\alpha_I \sinh(\alpha_P \lambda) + \alpha_P \cosh(\alpha_P \lambda)}{\alpha_P} e^{-\alpha_P \lambda} \right) + \frac{\alpha_I j_I}{\alpha_I^2 - \alpha_P^2} \left(1 - \frac{\alpha_I \cosh(\alpha_P \lambda) + \alpha_P \sinh(\alpha_P \lambda)}{\alpha_I} e^{-\alpha_P \lambda} \right), \quad (\text{A14})$$

$$Q = \left(Q_0 + \frac{\alpha_Q \alpha \cdot \mathbf{S}}{\alpha_P^2} (\cosh(\alpha_P \lambda) - 1) - I_0 \frac{\alpha_Q}{\alpha_P} \sinh(\alpha_P \lambda) \right) e^{-\alpha_I \lambda} + \frac{j_Q (1 - e^{-\alpha_I \lambda})}{\alpha_I} + \frac{(\alpha \cdot j) \alpha_Q}{\alpha_I (\alpha_I^2 - \alpha_P^2)} \left(1 - \left[\left(1 - \frac{\alpha_I^2}{\alpha_P^2} \right) - \frac{\alpha_I}{\alpha_P^2} (\alpha_I \cosh(\alpha_P \lambda) + \alpha_P \sinh(\alpha_P \lambda)) \right] e^{-\alpha_I \lambda} \right) + \frac{j_I \alpha_Q}{\alpha_P (\alpha_I^2 - \alpha_P^2)} \left(-\alpha_P + (\alpha_P \cosh(\alpha_P \lambda) + \alpha_I \sinh(\alpha_P \lambda)) e^{-\alpha_I \lambda} \right), \quad (\text{A15})$$

$$U = \left(U_0 + \frac{\alpha_U \alpha \cdot \mathbf{S}}{\alpha_P^2} (\cosh(\alpha_P \lambda) - 1) - I_0 \frac{\alpha_U}{\alpha_P} \sinh(\alpha_P \lambda) \right) e^{-\alpha_I \lambda} + \frac{j_U (1 - e^{-\alpha_I \lambda})}{\alpha_I} + \frac{(\alpha \cdot j) \alpha_U}{\alpha_I (\alpha_I^2 - \alpha_P^2)} \left(1 - \left[\left(1 - \frac{\alpha_I^2}{\alpha_P^2} \right) - \frac{\alpha_I}{\alpha_P^2} (\alpha_I \cosh(\alpha_P \lambda) + \alpha_P \sinh(\alpha_P \lambda)) \right] e^{-\alpha_I \lambda} \right) + \frac{j_I \alpha_U}{\alpha_P (\alpha_I^2 - \alpha_P^2)} \left(-\alpha_P + (\alpha_P \cosh(\alpha_P \lambda) + \alpha_I \sinh(\alpha_P \lambda)) e^{-\alpha_I \lambda} \right), \quad (\text{A16})$$

$$V = \left(V_0 + \frac{\alpha_V \alpha \cdot \mathbf{S}}{\alpha_P^2} (\cosh(\alpha_P \lambda) - 1) - I_0 \frac{\alpha_V}{\alpha_P} \sinh(\alpha_P \lambda) \right) e^{-\alpha_I \lambda} + \frac{j_V (1 - e^{-\alpha_I \lambda})}{\alpha_I} + \frac{(\alpha \cdot j) \alpha_V}{\alpha_I (\alpha_I^2 - \alpha_P^2)} \left(1 - \left[\left(1 - \frac{\alpha_I^2}{\alpha_P^2} \right) - \frac{\alpha_I}{\alpha_P^2} (\alpha_I \cosh(\alpha_P \lambda) + \alpha_P \sinh(\alpha_P \lambda)) \right] e^{-\alpha_I \lambda} \right) + \frac{j_I \alpha_V}{\alpha_P (\alpha_I^2 - \alpha_P^2)} \left(-\alpha_P + (\alpha_P \cosh(\alpha_P \lambda) + \alpha_I \sinh(\alpha_P \lambda)) e^{-\alpha_I \lambda} \right),$$

(A17)

where $\alpha_P^2 = \alpha_Q^2 + \alpha_U^2 + \alpha_V^2$, $\alpha \cdot \mathbf{S} = \alpha_Q Q_0 + \alpha_U U_0 + \alpha_V V_0$, and $\alpha \cdot j = \alpha_Q j_Q + \alpha_U j_U + \alpha_V j_V$. If we ignore emission only the first terms in (A14)-(A17) do not vanish. If $\alpha_P \rightarrow 0$ (or $\alpha_I \rightarrow 0$) then there is a danger of division by zero and one must take the appropriate limit analytically.

The general solution is found in a similar way (see LDI²). Because the matrix K_{AB} is not symmetric, the eigenvalues are complex, so there are both oscillatory and exponentially growing/decaying components to the solution.

This paper has been typeset from a T_EX/L^AT_EX file prepared by the author.